Title

Multifunctional self-priming hairpin probe-based isothermal nucleic acid amplification and its applications for COVID-19 diagnosis

Authors

Kim, Hansol
Lee, Seoyoung
Ju, Yong
et al.

Publication Date

2024-06-01

DOI

10.1016/j.bios.2024.116147

Biosensors and Bioelectronics 253 (2024) 116147

Contents lists available at ScienceDirect

Biosensors and Bioelectronics

journal homepage: www.elsevier.com/locate/bios

Multifunctional self-priming hairpin probe-based isothermal nucleic acid amplification and its applications for COVID-19 diagnosis

Hansol Kim [a,b], Seoyoung Lee [a], Yong Ju [a], Hyoyong Kim [a], Hyowon Jang [a,b], Yeonkyung Park [a,b], Sang Mo Lee [a], Dongeun Yong [c], Taejoon Kang [b,d,**], Hyun Gyu Park [a,*]

[a] Department of Chemical and Biomolecular Engineering (BK 21 four), Korea Advanced Institute of Science and Technology (KAIST), 291 Daehak-ro, Yuseong-gu, Daejeon, 34141, Republic of Korea

[b] Bionanotechnology Research Center, Korea Research Institute of Bioscience and Biotechnology (KRIBB), 125 Gwahak-ro, Yuseong-gu, Daejeon, 34141, Republic of Korea

[c] Department of Laboratory Medicine and Research Institute of Bacterial Resistance, Yonsei University College of Medicine, 50-1 Yonsei-ro, Seodaemun-gu, Seoul, 03722, Republic of Korea

[d] School of Pharmacy, Sungkyunkwan University, 2066 Seobu-ro, Jangan-gu, Suwon, Gyeonggi-do, 16419, Republic of Korea

ARTICLE INFO

Keywords:
Self-priming hairpin probe
Isothermal amplification
Molecular diagnostics
SARS-CoV-2
COVID-19

ABSTRACT

We herein present a multifunctional self-priming hairpin probe-based isothermal amplification, termed MSH, enabling one-pot detection of target nucleic acids. The sophisticatedly designed multifunctional self-priming hairpin (MSH) probe recognizes the target and rearranges to prime itself, triggering the amplification reaction powered by the continuously repeated extension, nicking, and target recycling. As a consequence, a large number of double-stranded DNA (dsDNA) amplicons are produced that could be monitored in real-time using a dsDNA-intercalating dye. Based on this unique design approach, the nucleocapsid (N) and the open reading frame 1 ab (ORF1ab) genes of SARS-CoV-2 were successfully detected down to 1.664 fM and 0.770 fM, respectively. The practical applicability of our method was validated by accurately diagnosing 60 clinical samples with 93.33% sensitivity and 96.67% specificity. This isothermal one-pot MSH technique holds great promise as a point-of-care testing protocol for the reliable detection of a wide spectrum of pathogens, particularly in resource-limited settings.

1. Introduction

Molecular diagnostics, notably exemplified during the COVID-19 pandemic, holds immense significance in swiftly and accurately identifying diseases, guiding treatment decisions, and tracking infectious outbreaks (Kim et al., 2024; Yuce et al., 2021). Polymerase chain reaction (PCR) is the gold standard method in molecular diagnostics by amplifying target nucleic acids through cycles of denaturation, annealing, and extension (Kifaro et al., 2022). However, PCR requires precisely controlled temperature cycling and expensive equipment, limiting its use in resource-limited settings. To overcome this limitation, several types of isothermal amplification techniques have been developed such as strand displacement amplification (SDA) (Shi et al., 2014), rolling circle amplification (RCA) (Lee et al., 2022), loop-mediated isothermal amplification (LAMP) (Soroka et al., 2021), nucleic acid sequence-based amplification (NASBA) (Cook, 2003), and exponential amplification reaction (EXPAR) (Lee et al., 2020; Reid et al., 2018). These methods typically require multiple primer sets, probes, and/or multiple enzymes to achieve isothermal amplification of target nucleic acids (Oliveira et al., 2021; Zhao et al., 2015).

Among them, strategies that utilize the combinatorial activities of nicking endonuclease and DNA polymerase, represented by EXPAR, have gained great attention because they could offer superior amplification capability over alternative methods (Cao et al., 2022). By taking advantage of the high amplification capability, the same amplifying approach has been also coupled into several conventional isothermal techniques. This has significantly improved the amplification efficiency by about 2–3 orders of magnitude, exemplified by the recently

* Corresponding author.
** Corresponding author. Bionanotechnology Research Center, Korea Research Institute of Bioscience and Biotechnology (KRIBB), 125 Gwahak-ro, Yuseong-gu, Daejeon, 34141, Republic of Korea.
E-mail addresses: kangtaejoon@kribb.re.kr (T. Kang), hgpark@kaist.ac.kr (H.G. Park).

https://doi.org/10.1016/j.bios.2024.116147
Received 23 December 2023; Received in revised form 12 February 2024; Accepted 19 February 2024
Available online 20 February 2024

developed nicking and extension chain reaction system-based amplification (NESBA) (Ju et al. 2021, 2022) and netlike rolling circle amplification (NRCA) (Song et al., 2022; Zhu et al., 2015) techniques. However, these strategies still require multiple primers and/or high reaction temperatures, leaving considerable room for the development of more advanced methods.

A hairpin structure is a specific type of DNA secondary structure formed by a loop of single-stranded nucleic acid and a self-complementary double-stranded stem region. In the field of nucleic acid detection, hairpin structures have proven to be multifunctional, recognizing target nucleic acids and also initiating subsequent secondary reactions. Hairpin-based approaches typically depend on a process where the hairpin structure unfolds as the target nucleic acid binds to the loop region, triggering the intended reactions in the now accessible stem region (Kim et al., 2020; Li et al., 2022; Song et al., 2020). Since the hybridized stem region provides structural constraints on the hairpin opening, more stringent complementarity is required for the binding between the loop and target sequences, consequently resulting highly enhanced specificity (Bonnet et al., 1999). These properties have led to the advancement of hairpin-based biosensing technology, represented by catalytic hairpin assembly and hybridization chain reaction (Do et al., 2021; Kim et al., 2020; Zhang et al., 2023). The methods have become a critical platform for the specific detection of target nucleic acids and have achieved success in the diagnosis of COVID-19 (Karami et al., 2021; Kashefi-Kheyrabadi et al., 2022).

Based on this background, we developed a multifunctional self-priming hairpin probe-based isothermal amplification (MSH) method powered by the hairpin structure and the amplification through the combined activities of nicking enzyme and DNA polymerase. Moreover, we successfully applied this technique to identify SARS-CoV-2 genomic RNA (gRNA) as a model target under an isothermal condition.

2. Experimental section

2.1. Materials

All DNA oligonucleotides used in this study were synthesized and polyacrylamide gel electrophoresis (PAGE)-purified by Genotech Co. (Daejeon, Republic of Korea). RNA oligonucleotides were synthesized and high-performance liquid chromatography (HPLC)-purified by IDT (Coralville, IA, USA). The oligonucleotide sequences are listed in Table S1. Klenow Fragment DNA Polymerase (exo-) (KF) and 10 × KF buffer (100 mM Tris-HCl, 100 mM $MgCl_2$, 10 mM dithiothreitol (DTT), 500 mM NaCl, pH 7.9) were purchased from Enzynomics (Daejeon, Republic of Korea). Nt.AlwI, 10 × CutSmart buffer (200 mM Tris-acetate (Ac), 500 mM KAc, 100 mM $Mg(Ac)_2$, 1 mg/mL bovine serum albumin (BSA) (pH 7.9), and deoxynucleotide solution mixture (dNTPs) were purchased from New England Biolabs Inc. (Beverly, MA, USA). 10000 × SYBR Green I was purchased from Invitrogen (Carlsbad, CA, USA). The gRNAs of SARS-CoV-2 (BetaCoV/Korea/KCDC03/2020), Middle East respiratory syndrome coronavirus (MERS-CoV), and human coronavirus (HCoV) NL63 (HCoV-NL63) were provided by the National Culture Collection for Pathogens (NCCP) (Cheongju, Republic of Korea), and those of HCoV-229E, HCoV-OC43, respiratory syncytial virus (RSV), and influenza A virus subtype H3N2 (H3N2) were purchased from the Korea Bank for Pathogenic Viruses (KBPV) (Seoul, Republic of Korea). Ultrapure DNase/RNase-free distilled water (DW) was purchased from Bioneer® (Daejeon, Republic of Korea) and used in all the experiments. All other chemicals were of analytical grade and were used without further purification.

2.2. MSH protocols to detect SARS-CoV-2

To confirm that the designed MSH probe could form a stable and intended hairpin structure at 37 °C, the secondary structures and Gibbs free energy changes of the probe were monitored using Oligo Analyzer version 3.1 (IDT). 20 μL of MSH reaction solutions were prepared by mixing 2 μL of MSH probe (1 μM), 2 μL of dNTPs (2.5 mM each), 1 μL of 20 × SYBR Green I, 0.5 μL of KF (5 U/μL), 0.4 μL of Nt.AlwI (10 U/μL), 10.1 μL of DW, and 2 μL of target RNA. The solution was then incubated at 37 °C, and the fluorescence signal of SYBR Green I was monitored at 30 s intervals using a CFX Connect™ Real-Time System (Bio-Rad, Hercules, CA, USA).

2.3. PAGE analysis and melting curve analysis

For PAGE analysis, a 10 μL aliquot of the reaction solution was mixed with 2 μL of 6 × loading buffer (Bioneer®) and run on a 15% polyacrylamide gel at a constant voltage of 120 V for 90 min using 1 × tris/borate/ethylenediaminetetraacetic acid (TBE) as the running buffer. After GelRed staining for 15 min, the gel image was captured using a ChemiDoc™ Imaging System (Bio-Rad). For melting curve analysis, 20 μL of the reaction components or products containing 1 × SYBR Green I were heated at 37 °C for 10 min. The fluorescence signal was measured using a CFX Connect™ Real-Time System (Bio-Rad) by increasing the temperature to 90 °C in 0.5 °C increments every 5 s. The first derivative of the fluorescence curve [-d(RFU)/dT] was used to determine the melting temperature.

2.4. COVID-19 testing of clinical samples

A total of 60 clinical samples (43 nasopharyngeal swabs and 17 sputa) were collected from individuals suspected of having SARS-CoV-2 infection and placed in Universal Transport Medium (Asanpharm, Seoul, Republic of Korea) by Severance hospital (IRB approval number: 4-2020-0465; Seoul, Republic of Korea). The gRNAs of clinical samples were extracted using the AdvanSure™ Nucleic Acid R Kit (LG chem, Seoul, Republic of Korea). 2 μL of the extracted gRNAs were subjected to the MSH reaction as described above.

Quantitative reverse transcription PCR (qRT-PCR) was performed using Allplex™ 2019-nCoV assay Kit (Seegene, Seoul, Republic of Korea). RT was performed at 50 °C for 20 min, followed by denaturation at 95 °C for 15 min. Then, PCR was performed by 45 cycles of 15 s at 94 °C and 30 s at 58 °C. The fluorescence signal was measured at each cycle using a CFX Connect™ Real-Time System (Bio-Rad). Diagnostic decisions were made for each clinical sample based on the C_t values (i.e., threshold cycle) determined by the embedded system software.

3. Results and discussion

3.1. Operating principle of the MSH reaction

As illustrated in Fig. 1, the MSH probe employed as a key component in this work is a hairpin structure extended by overhangs at both the 3′ and 5′ ends. The target is recognized by the two target-complementary domains (blue) located at the 5′ overhang and the loop, separated by the target-independent stem region (purple). The hairpin loop also contains the complement (RS*) of Nt.AlwI recognition sequence (RS; 5′-**GGATC**NNNN$^{\downarrow}$N-3′) (thick black). The 3′ overhang is the self-priming tail (red), which would fold back to initiate an extension reaction upon opening of the hairpin due to its complementarity with the part of stem. At the reaction temperature of 37 °C, the closed hairpin structure with a 14 base-pair (bp) stem (structure A with ΔG of −11.44 kcal/mol in Fig. S1) is more stable than the opened fold-back structure with 6 bp complementarity (structure A′ with ΔG of −6.95 kcal/mol in Fig. S1). Thus, structure A keeping the closed hairpin structure is the predominant form of MSH under the reaction condition, preventing the self-priming and subsequent non-specific enzymatic reactions without a target.

When target RNA is present, it binds to the two target recognition regions of the MSH probe, causing a rearrangement of the hairpin structure and exposing the hairpin stem, which would allow the self-

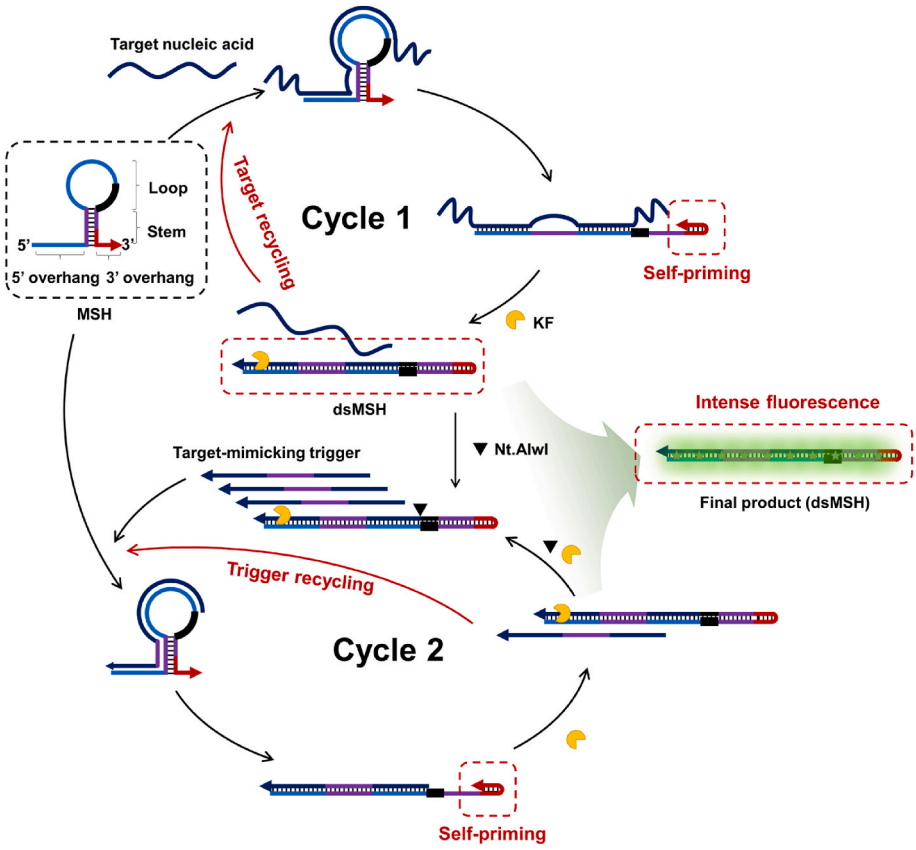

Fig. 1. Schematic illustration of the MSH method for target nucleic acid detection.

priming tail to fold back. KF then extends the fold-backed 3' end of the MSH probe, producing a double-stranded DNA product (dsMSH) and concomitantly displacing the hybridized target nucleic acid. The released target is then recycled and participates in another MSH opening reaction (cycle 1). Since the dsMSH is to contain a double-stranded Nt.AlwI recognition site, repeated cycles of cleavage and extension reactions would be promoted from the dsMSH through the combined activities of KF and Nt.AlwI. As a result, a large number of target-mimicking triggers are produced, which could trigger other MSH opening reactions through binding to free MSH probes like the original target nucleic acids, further accelerating the amplification reaction (cycle 2). These interconnected iterative reactions finally produce a large number of dsMSH that could be monitored in real-time by a double-stranded DNA (dsDNA)-specific fluorescent dye (SYBR Green I), allowing one-pot detection of the target nucleic acid under isothermal conditions.

In the MSH probe, the stem sequence is kept constant to maintain stable amplification efficiency regardless of the target sequence. The hairpin structure has two distinct target recognition sites: one in the loop and another at the 5′ overhang. The interaction of the loop with the target is critical for changing the configuration of the hairpin, while the 5' overhang helps to align the target sequence without independently initiating the opening of the hairpin (Fig. S2). This design ensures that the reaction is effectively triggered by the presence of target RNA, as evidenced by the lower ΔG value for the full-length target interaction compared to loop-only binding.

3.2. Feasibility of the MSH reaction

To verify the feasibility of the MSH approach, the sequence from the SARS-CoV-2 N gene was selected as a model target. Comparative experiments were then performed under different combinations of reaction components. As shown in Fig. 2a, a significant increase in fluorescence signal was observed only in the sample containing all reaction components, including MSH, KF, Nt.AlwI, and target RNA (curve 2). In contrast, a negligible fluorescence signal was observed when the target RNA was excluded (curve 1). When any one of the reaction components (MSH, KF, and Nt.AlwI) was missing, the fluorescence enhancement was negligible even in the presence of the target RNA (curves 3, 4, and 5). We also examined the two control hairpin probes having the same target recognition sequence as the MSH probe but without the 3′ tail or with a random 3' tail sequence (Fig. S3), which are supposed to lack the ability to promote self-priming rearrangement. As expected, only negligible fluorescence signals were observed in these cases (Figs. S3b and c). All these results confirm that the MSH reaction was properly initiated by the target RNA and operated to produce the fluorescence signals with the cooperation of all the reaction components including the uniquely designed MSH probe capable of self-priming in the presence of the target.

Next, we performed PAGE analysis of the reaction components and products (Fig. 2b). M1–5 are the lanes for MSH probe, synthetic target RNA, target-mimicking trigger, MSH probe complexed with target, and MSH probe complexed with trigger, respectively. Lane 1 shows bands from all reaction components, including MSH, KF, and Nt.AlwI but without target RNA. As expected, there was no band observed for the final product, dsMSH in this case, but a weak band slightly below the dsMSH band was observed that is assumed to be the band for the MSH/trigger duplex (M5 lane), indicating that the MSH probe might be slightly opened and a marginal amount of target-mimicking trigger could be produced even without the target. In the presence of target RNA together with MSH, KF, and Nt.AlwI (lane 2), three bands corresponding to dsMSH (green box), recycled free target RNA (red box), and target-mimicking trigger (navy box) were clearly observed, but the band for the MSH probe almost disappeared, indicating that all the applied

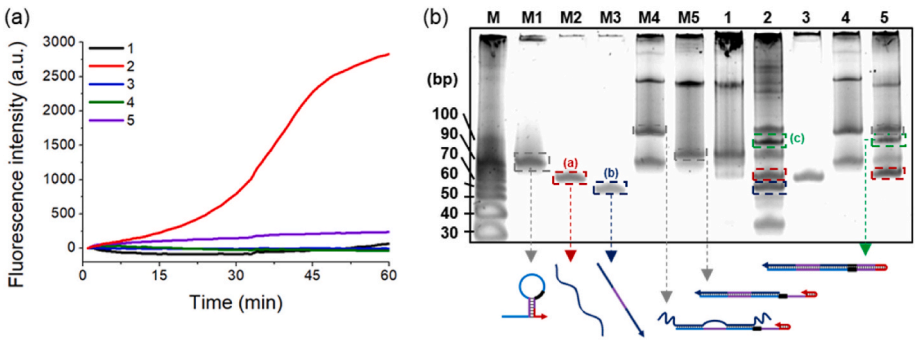

Fig. 2. Feasibility of the MSH method. (a) Real-time fluorescence curves during the MSH reactions under various reaction components (1: MSH probe + KF + Nt.AlwI, 2: MSH probe + KF + Nt.AlwI + target RNA, 3: KF + Nt.AlwI + target RNA, 4: MSH probe + Nt.AlwI + target RNA, 5: MSH probe + KF + target RNA). The final concentrations of target RNA, MSH probe, KF, and Nt.AlwI are 5 nM, 50 nM, 0.125 U/μL, and 0.5 U/μL, respectively. (b) PAGE image of the MSH products (M: 10 bp DNA ladder, M1: MSH probe, M2: target RNA, M3: target-mimicking trigger, M4: MSH probe + target RNA, M5: MSH probe + target-mimicking trigger, 1: MSH probe + KF + Nt.AlwI, 2: MSH probe + KF + Nt.AlwI + target RNA, 3: KF + Nt.AlwI + target RNA, 4: MSH probe + Nt.AlwI + target RNA, 5: MSH probe + KF + target RNA). The final concentrations of target RNA, MSH probe, KF, and Nt.AlwI are 100 nM, 100 nM, 100 nM, 0.125 U/μL, and 0.5 U/μL, respectively.

MSH probes are already involved in the reactions. We also examined the band patterns of the negative controls omitting one of the key components: MSH (lane 3), KF (lane 4), and Nt.AlwI (lane 5). Our observations confirmed the absence of the target-mimicking trigger band, a key product, in all these lanes. The band for dsMSH, indicating the final product, was observed in lane 5 as a result of the target-induced self-priming event but its amount was lower than that in lane 2, suggesting its slower reaction rate compared to the reaction accelerated by Nt.AlwI. Overall, the PAGE analysis concretely supports the real-time fluorescence results and confirms that the MSH method works as proposed in Fig. 1.

In addition, we conducted a melting curve analysis of the products (Fig. S4) after 10 min of the MSH reaction in the presence (red) and absence (black) of target RNA (Fig. S4c). As a result, two distinct peaks, corresponding to the MSH/trigger (T_m = 81 °C) and dsMSH (T_m = 86 °C), were observed only from the sample containing the target RNA, further confirming the proper operation of the MSH reaction.

3.3. Sensitivity and selectivity of the MSH reaction

To maximize the efficiency of the MSH reaction, we conducted an optimization of various reaction conditions including the length of the self-priming tail, the concentrations of MSH probe and enzymes, and the reaction temperature. The optimization was performed by comparing

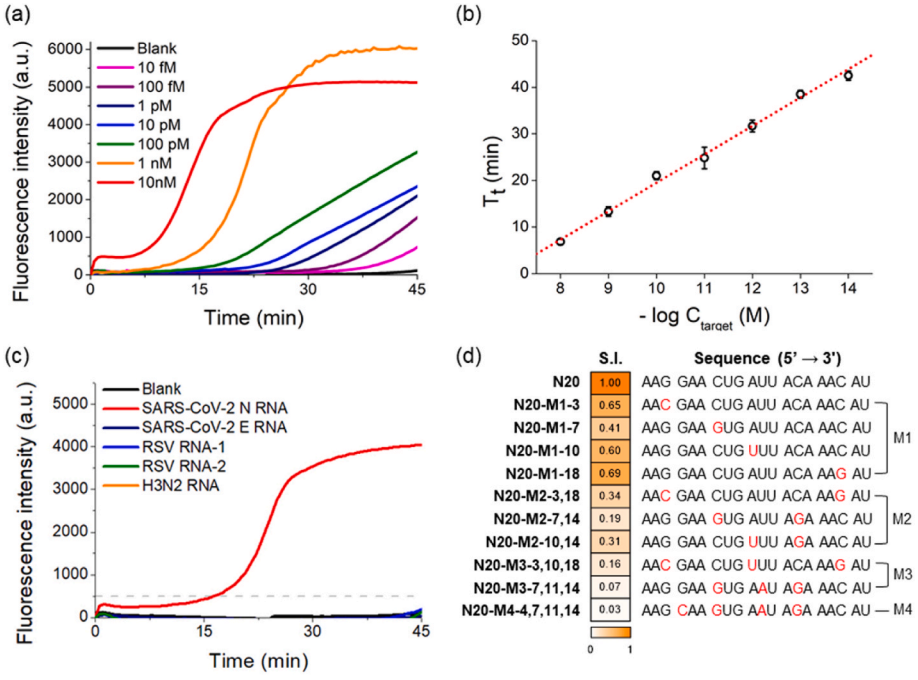

Fig. 3. Sensitivity and selectivity of the MSH method for the detection of SARS-CoV-2 N RNA. (a) Real-time fluorescence curves during the MSH reactions over a range of target RNA concentrations from 10 fM to 10 nM. Threshold line (fluorescence intensity = 500 a.u.) is marked as gray dashed line. (b) Plot of T_t value against the logarithm of target RNA concentration (C_{target}). T_t is defined as the reaction time at which the real-time fluorescence signal crosses the threshold line in Fig. 3a. Red dotted line is linear fit. Error bars were determined from triplicate measurements. (c) Real-time fluorescence curves during the MSH reactions with target (SARS-CoV-2 N RNA) and non-target RNAs (SARS-CoV-2 E, RSV-1, RSV-2, and H3N2 RNAs) (C_{target} and $C_{non\text{-}target}$ = 1 nM). Threshold line is marked as gray dashed line. (d) Specificity of the MSH reaction with non-target RNAs exhibiting few mismatches (C_{target} and $C_{non\text{-}target}$ = 1 nM). The specificity index (S.I.) is defined as 1-[(T_t(MM)-T_t(PM))/T_t(PM)], where the T_t(PM) and T_t(MM) are the threshold times from the samples containing perfectly matched target RNA and mismatched target RNA. The S.I. values are visually represented as a heatmap. In the label N20-Mx-y, 'x' indicates the number of mismatches, and 'y' specifies the sites of mismatches. Mismatches within the sequence are indicated in red.

the real-time fluorescence signals obtained from the reaction mixtures with target RNA to those obtained from the reaction mixtures without target RNA. The threshold time (T_t) was defined as the reaction time at which the real-time fluorescence signal crossed the threshold line (500 a.u.). We focused on maximizing the difference in T_t values between the positive signal and the background signal, while reducing the overall reaction time with faster amplification. As a result, the optimal conditions for the MSH method were selected as 6-mer self-priming tail, 50 nM MSH probe, 0.125 U/μL KF, 0.2 U/μL Nt.AlwI, and reaction temperature of 37 °C (Figs. S5–9). It is noteworthy that the length of the self-priming tail is crucial for effective initiation of the MSH reaction. The results indicated that a 6-mer tail provided optimal amplification efficiency. Shorter tails were less efficient in amplification, while the 7-mer tail resulted in a rapid, indistinct background signal, likely due to the formation of secondary hairpin structures even in the absence of target RNA.

To determine the sensitivity of the MSH strategy, we monitored real-time fluorescence signals from the MSH reaction over a range of target RNA concentrations from 10 fM to 10 nM (Fig. 3a). The plot of T_t value against the logarithm of target RNA concentration (C_{target}) showed an excellent linear relationship ($T_t = -6 \log C_{target} - 40.476$, $R^2 = 0.995$), allowing for the quantitative detection of target RNA (Fig. 3b). The limit of detection (LOD) was determined to be 16.57 fM using the formula (limit of blank (LOB) = mean of blank + 1.645 × standard deviation of blank, LOD = LOB + 1.645 × standard deviation of lowest concentration sample) (Armbruster and Pry, 2008). This LOD is comparable to or better than previous isothermal amplification methods (Table S2).

The specificity of the MSH reaction was also evaluated by comparing the fluorescence signals from the target SARS-CoV-2 N gene with several non-target synthetic RNAs of the SARS-CoV-2 envelope (E) gene, RSV, and H3N2 (Table S1). The results showed that a highly enhanced fluorescence signal was produced only from the target RNA (red curve in Fig. 3c) while fluorescence signals from non-target RNAs or the negative control were negligible (navy, blue, green, yellow, and black curves in Fig. 3c), verifying the excellent specificity of the MSH method. We further evaluated the specificity of the MSH method against mismatched target RNAs (Fig. 3d and S10). Fig. S10a shows that a 20 nt RNA (N20) resulted in a delayed fluorescence response (higher T_t value) compared to the full-length sequence (N60), likely due to the lower affinity of N20 for the MSH probe. To quantitatively assess specificity, we introduced a specificity index (S.I.), defined as 1 - [(T_t(MM) - T_t(PM))/T_t(PM)], comparing threshold times for perfectly matched (PM) and mismatched (MM) target RNAs. Mismatches resulted in reduced S.I. values, indicating slower probe opening. In particular, a cytosine mismatch at position 7 significantly affected specificity, as shown by variants N20-M1-7, N20-M2-7, 14, and N20-M3-7, 11, 14 in Fig. 3d. These results confirm the ability of the MSH method to accurately identify the target sequence even with minor mismatches.

3.4. MSH reaction for COVID-19 diagnosis

To verify the practical capability of the MSH method, it was applied to detect two genes from SARS-CoV-2 gRNA: N and ORF1ab (Fig. 4a). The ORF1ab and N genes are frequently targeted for COVID-19 detection due to their important roles in the viral replication and structure. These regions have been found to persist longer in COVID-19 positive patients compared to other viral genes, making them reliable targets for detection assays (Zhou et al., 2020; Zhu et al., 2022). First, the MSH probe targeting N gene was employed to detect SARS-CoV-2 gRNA, which showed that T_t values correctly decreased with increasing concentrations of SARS-CoV-2 gRNA (C_{target}) (Fig. 4b). The plot of T_t value against the logarithm of C_{target} showed an excellent linear relationship ($T_t = -6.85 \log C_{target} - 58.3$, $R^2 = 0.997$) with an LOD of 1.664 fM. Next, we designed another MSH probe to detect ORF1ab gene (MSH-ORF1ab) simply by putting the ORF1ab gene-specific sequence to the loop while keeping the same stem and 3' overhang sequences with the N gene. As shown in Fig. 4c, the MSH reaction also successfully identified the ORF1ab gene of SARS-CoV-2 gRNA down to 0.770 fM yielding an excellent linear relationship ($T_t = -6.55 \log C_{target} - 54.87$, $R^2 = 0.985$). Like this, the MSH reaction could be easily adaptable to the detection of different target sequences by simply modifying only the target recognition regions of the MSH probe. Next, the specificity of the MSH method against gRNAs from different viruses was evaluated. Fig. 4d shows that a highly enhanced fluorescence signal was observed only from the target SARS-CoV-2 gRNA, while the fluorescence signals from the non-target viruses such as MERS-CoV, HCoV-NL63, HCoV-229E, HCoV-OC43, RSV, and H3N2 were negligible. These results confirmed the exceptional specificity of the MSH system in identifying target SARS-CoV-2 gRNA.

The faster amplification observed with gRNA compared to synthetic RNA targets is an interesting phenomenon. This difference becomes less pronounced at lower target concentrations, suggesting that non-target sequences within the gRNA may inadvertently facilitate the opening of

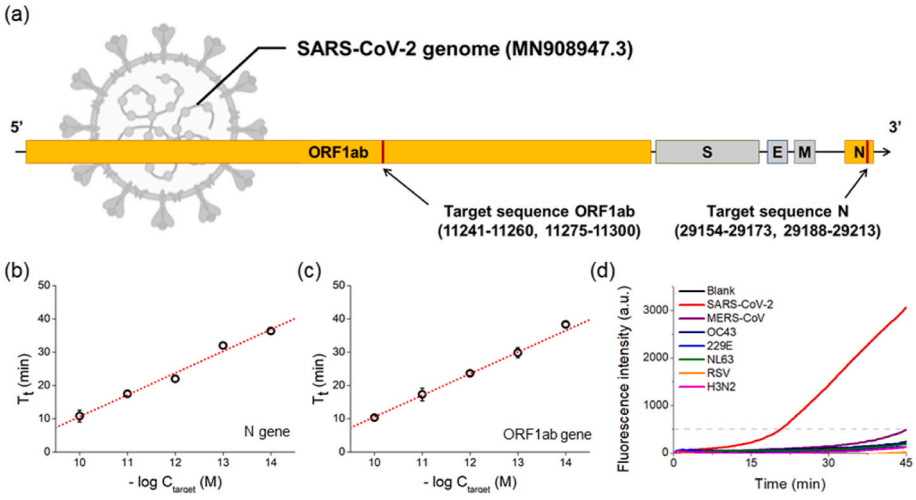

Fig. 4. Detection of SARS-CoV-2 gRNA using the MSH method. (a) Target sequences of SARS-CoV-2 N and ORF1ab genes. The SARS-CoV-2 genome based on NCBI sequence MN908947.3 was used. (b, c) Plots of T_t value against the logarithm of SARS-CoV-2 gRNA concentration (C_{target}) when targeting (b) N and (c) ORF1ab genes, respectively. Error bars represent the standard deviation from triplicate measurements. The red dotted lines indicate linear fits. (d) Real-time fluorescence curves during the MSH reactions with target (SARS-CoV-2 gRNA) and non-target gRNAs (MERS-CoV, HCoV-OC43, HCoV-229E, HCoV-NL63, RSV, and H3N2) (C_{target} and $C_{non\text{-}target}$ = 10 pM).

the hairpin structure in a dense molecular environment. In addition, the use of carrier RNA during gRNA extraction may also contribute to this acceleration by interacting with the gRNA sequences to promote hairpin opening. However, as shown in Fig. 4d, the lack of amplification with other gRNAs confirms the specificity of the MSH method for SARS-CoV-2 gRNA.

Finally, the clinical potential of the MSH method was assessed by detecting the SARS-CoV-2 N gene in 60 clinical samples including nasopharyngeal swabs (NPS) and sputum samples. As illustrated in Fig. 5a, RNA was extracted from the collected clinical samples and subjected to the MSH reaction. For this study, we introduced a new variable, '45-T_t' to represent the amount of SARS-CoV-2. If the fluorescence intensity does not reach the threshold line even after 45 min of the MSH reaction, the 45 - T_t value was assigned as zero. The experimental result was visually depicted as a heatmap in Fig. 5b and quantitatively presented as a scatter plot in Fig. 5c. Both Fig. 5b and c depicted a pronounced distinction between the positive and negative groups, in alignment with qRT-PCR results, with a significant statistical p-value ($p < 0.0001$). Receiver operating characteristic (ROC) curve analysis was used to evaluate the ability of the MSH method to discriminate between positive and negative samples. The analysis revealed an area under the curve (AUC) of 0.9489 ± 0.034 with a 95% confidence interval (CI) of 0.8823–1.000 and a p-value of less than 0.0001 (Fig. 5d). This AUC value is considered indicative of high diagnostic accuracy (Carter et al., 2016). Using Youden's index (Fluss et al., 2005), we determined an optimal cut-off point of 7, at which the MSH method achieved a sensitivity of 93.33% and a specificity of 96.67%, further confirming the high diagnostic accuracy of the method.

4. Conclusion

The MSH method offers several advantages over existing isothermal nucleic acid detection techniques. First, the MSH method requires only a single hairpin probe, contrary to many previous isothermal amplification methods that require multiple primers (Table S2). This simplicity is due to the probe's self-priming tail acting as a primer, reducing the complexity of the reaction and lowering non-specific background signals. Second, sensitive target detection is achieved through the continuous recycling of target nucleic acid by the self-priming tail extension-mediated strand displacement. The production of target-mimicking triggers further boosts amplification, resulting in the limit of detection (LOD) of the MSH method being comparable to or better than that of previous isothermal amplification methods (Table S2). Third, the modular design of the MSH probe allows for easy adaptation to different

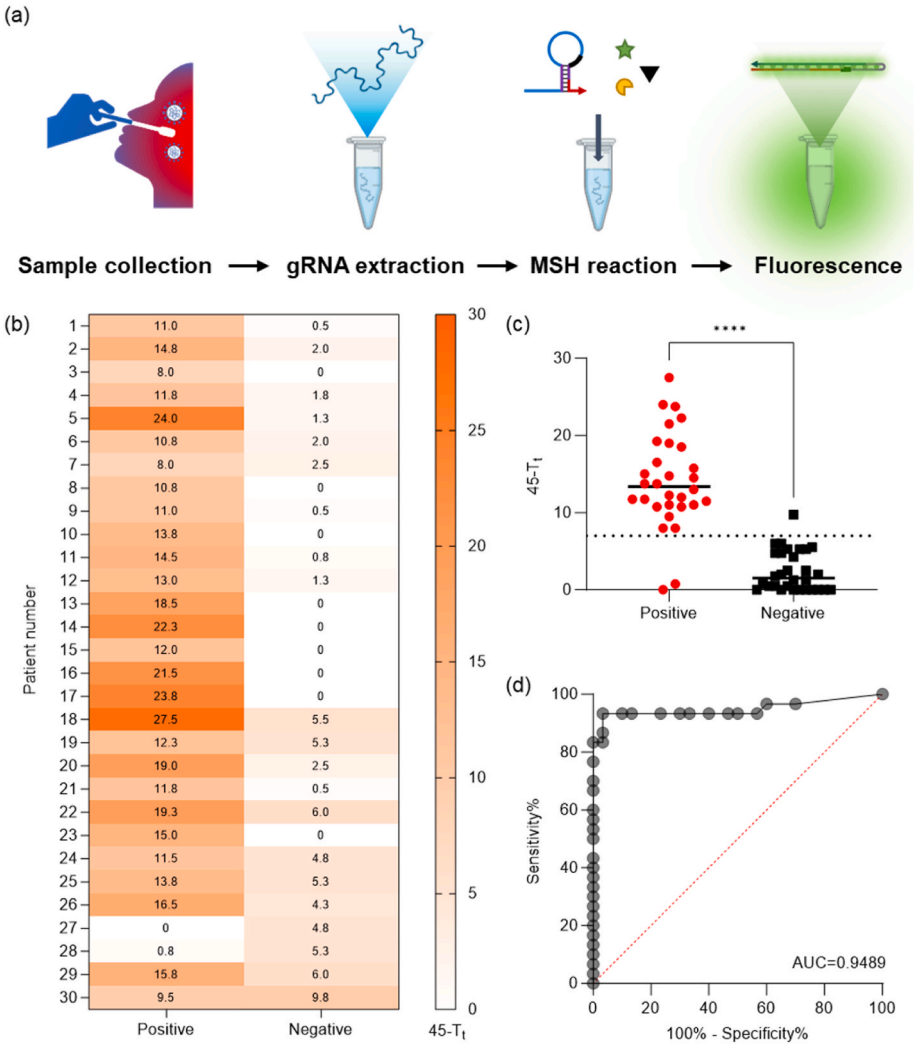

Fig. 5. MSH reaction for COVID-19 diagnosis. (a) Schematic illustration of COVID-19 diagnosis using the MSH method. (b) Heatmap of 45 - T_t values obtained by MSH reactions of 60 clinical samples. (c) Scatter plot of 45 - T_t values obtained by MSH reactions in the positive (N = 30) and negative (N = 30) group (n = 2, $p < 0.0001$; two-tailed Student's t-test with Welch's correction). (d) ROC curve evaluating performance of MSH with 30 positive and 30 negative clinical samples. ROC analysis was performed with the standard parameters in Prism 10, using Wilson/Brown method for CI calculation. All statistical analyses were performed at 95% confidence level.

target sequences by simply changing the target recognition region while preserving the other sequences. We successfully detected the N and ORF1ab genes of SARS-CoV-2 using the MSH method with the different MSH probes. Additionally, the probe's two separate target recognition domains ensure high specificity, as the reaction initiates only when the target properly hybridizes with both the 5′ overhang and the loop of the MSH probe. These features enabled the MSH method to diagnose COVID-19 in 60 clinical samples with a 93.33% sensitivity and 96.67% specificity. We anticipate that the MSH method, as presented here, can find broad applications in the detection of diverse nucleic acids, making significant contributions to fields such as disease diagnosis, environmental monitoring, food safety, forensics, and beyond.

CRediT authorship contribution statement

Hansol Kim: Writing – review & editing, Writing – original draft, Visualization, Software, Resources, Project administration, Methodology, Investigation, Funding acquisition, Formal analysis, Data curation, Conceptualization. **Seoyoung Lee:** Writing – review & editing, Resources, Methodology, Investigation. **Yong Ju:** Resources, Methodology, Investigation. **Hyoyong Kim:** Resources, Methodology, Investigation. **Hyowon Jang:** Resources, Investigation. **Yeonkyung Park:** Writing – review & editing. **Sang Mo Lee:** Resources. **Dongeun Yong:** Resources. **Taejoon Kang:** Writing – review & editing, Supervision, Project administration, Funding acquisition. **Hyun Gyu Park:** Writing – review & editing, Supervision, Funding acquisition.

Declaration of competing interest

The authors declare that they have no known competing financial interests or personal relationships that could have appeared to influence the work reported in this paper.

Data availability

Data will be made available on request.

Acknowledgement

This research was supported by National Research Foundation of Korea (NRF) grants funded by Korea government (MSIT) (NRF-2021R1A2B5B03001739, NRF-2021M3E5E3080379, NRF-2021M3H4A1A02051048, and NRF-2023R1A2C2005185), Basic Science Research Program funded by Korea government (MOE) (RS-2023-00273434), Technology Development Program for Biological Hazards Management in Indoor Air through KEITI funded by Korea government (ME) (2021003370003), KEIT grant funded by Korea government (MOTIE) (RS-2022-00154853), Nanomedical Devices Development Program of National Nano Fab Center (NNFC) (CSM2105M101), and KRIBB Research Initiative Program (KGM5472413).

Appendix A. Supplementary data

Supplementary data to this article can be found online at https://doi.org/10.1016/j.bios.2024.116147.

References

Armbruster, D.A., Pry, T., 2008. Limit of blank, limit of detection and limit of quantitation. Clin. Biochem. Rev. 29, S49–S52.

Bonnet, G., Tyagi, S., Libchaber, A., Kramer, F.R., 1999. Thermodynamic basis of the enhanced specificity of structured DNA probes. Proc. Natl. Acad. Sci. U.S.A. 96 (11), 6171–6176.

Cao, S., Tang, X., Chen, T., Chen, G., 2022. Types and applications of nicking enzyme-combined isothermal amplification. Int. J. Mol. Sci. 23 (9).

Carter, J.V., Pan, J., Rai, S.N., Galandiuk, S., 2016. ROC-ing along: evaluation and interpretation of receiver operating characteristic curves. Surgery 159 (6), 1638–1645.

Cook, N., 2003. The use of NASBA for the detection of microbial pathogens in food and environmental samples. J. Microbiol. Methods 53 (2), 165–174.

Do, J.Y., Jeong, J.Y., Hong, C.A., 2021. Catalytic hairpin DNA assembly-based chemiluminescent assay for the detection of short SARS-CoV-2 target cDNA. Talanta 233, 122505.

Fluss, R., Faraggi, D., Reiser, B., 2005. Estimation of the Youden Index and its associated cutoff point. Biomet. J.: J. Math. Meth. Biosci. 47 (4), 458–472.

Ju, Y., Kim, H.Y., Ahn, J.K., Park, H.G., 2021. Ultrasensitive version of nucleic acid sequence-based amplification (NASBA) utilizing a nicking and extension chain reaction system. Nanoscale 13 (24), 10785–10791.

Ju, Y., Kim, J., Park, Y., Lee, C.Y., Kim, K., Hong, K.H., Lee, H., Yong, D., Park, H.G., 2022. Rapid and accurate clinical testing for COVID-19 by nicking and extension chain reaction system-based amplification (NESBA). Biosens. Bioelectron. 196, 113689.

Karami, A., Hasani, M., Azizi Jalilian, F., Ezati, R., 2021. Hairpin-spherical nucleic acids for diagnosing COVID-19: a simple method to generalize the conventional PCR for molecular assays. Anal. Chem. 93 (26), 9250–9257.

Kashefi-Kheyrabadi, L., Nguyen, H.V., Go, A., Baek, C., Jang, N., Lee, J.M., Cho, N.H., Min, J., Lee, M.H., 2022. Rapid, multiplexed, and nucleic acid amplification-free detection of SARS-CoV-2 RNA using an electrochemical biosensor. Biosens. Bioelectron. 195, 113649.

Kifaro, E.G., Kim, M.J., Jung, S., Noh, J.Y., Song, C.S., Misinzo, G., Kim, S.K., 2022. Direct reverse transcription real-time PCR of viral RNA from saliva samples using hydrogel microparticles. Biochip. J. 16 (4), 409–421.

Kim, H.Y., Ahn, J.K., Lee, C.Y., Park, H.G., 2020. A hairpin probe-mediated isothermal amplification method to detect target nucleic acid. Anal. Chim. Acta 1114, 7–14.

Kim, H., Jang, H., Song, J., Lee, S.M., Lee, S., Kwon, H.J., Park, H.G., 2024. A CRISPR/Cas12 trans-cleavage reporter enabling label-free colorimetric detection of SARS-CoV-2 and its variants. Biosens. Bioelectron., 116102

Lee, H.N., Lee, J., Kang, Y.K., Lee, J.H., Yang, S., Chung, H.J., 2022. A lateral flow assay for nucleic acid detection based on rolling circle amplification using capture ligand-modified oligonucleotides. Biochip. J. 16 (4), 441–450.

Lee, S., Jang, H., Kim, H.Y., Park, H.G., 2020. Three-way junction-induced isothermal amplification for nucleic acid detection. Biosens. Bioelectron. 147, 111762.

Li, Y., Kim, H., Ju, Y., Park, Y., Kang, T., Yong, D., Park, H.G., 2022. Ultrasensitive isothermal detection of SARS-CoV-2 based on self-priming hairpin-utilized amplification of the G-rich sequence. Anal. Chem. 94 (50), 17448–17455.

Oliveira, B.B., Veigas, B., Baptista, P.V., 2021. Isothermal amplification of nucleic acids: the race for the next "gold standard.". Frontier. Sens. 2.

Reid, M.S., Le, X.C., Zhang, H., 2018. Exponential isothermal amplification of nucleic acids and assays for proteins, cells, small molecules, and enzyme activities: an EXPAR example. Angew Chem. Int. Ed. Engl. 57 (37), 11856–11866.

Shi, C., Liu, Q., Ma, C., Zhong, W., 2014. Exponential strand-displacement amplification for detection of microRNAs. Anal. Chem. 86 (1), 336–339.

Song, J.Y., Jung, Y., Lee, S., Park, H.G., 2020. Self-priming hairpin-utilized isothermal amplification enabling ultrasensitive nucleic acid detection. Anal. Chem. 92 (15), 10350–10356.

Song, Y., Chao, Y., Guo, Y., Zhang, F., Mao, C., Guan, C., Chen, G., Feng, C., 2022. Paper-based netlike rolling circle amplification (NRCA) for ultrasensitive and visual detection of SARS-CoV-2. Sensor. Actuator. B Chem. 358, 131460.

Soroka, M., Wasowicz, B., Rymaszewska, A., 2021. Loop-mediated isothermal amplification (LAMP): the better sibling of PCR? Cells 10 (8).

Yuce, M., Filiztekin, E., Ozkaya, K.G., 2021. COVID-19 diagnosis -A review of current methods. Biosens. Bioelectron. 172, 112752.

Zhang, Y., Huang, X., Li, W., Xie, Q., Zhang, J., Luo, F., Qiu, B., Chen, Z., Lin, Z., Xu, G., 2023. Dual-target nucleic acid sequences responsive electrochemiluminescence biosensor using single type carbon dots as probe for SARS-CoV-2 detection based on series catalytic hairpin assembly amplification. Sensor. Actuator. B Chem. 379, 133223.

Zhao, Y., Chen, F., Li, Q., Wang, L., Fan, C., 2015. Isothermal amplification of nucleic acids. Chem. Rev. 115 (22), 12491–12545.

Zhou, Y., Pei, F., Ji, M., Wang, L., Zhao, H., Li, H., Yang, W., Wang, Q., Zhao, Q., Wang, Y., 2020. Sensitivity evaluation of 2019 novel coronavirus (SARS-CoV-2) RT-PCR detection kits and strategy to reduce false negative. PLoS One 15 (11), e0241469.

Zhu, X., Feng, C., Zhang, B., Tong, H., Gao, T., Li, G., 2015. A netlike rolling circle nucleic acid amplification technique. Analyst 140 (1), 74–78.

Zhu, X., Zhou, F., Zhou, Q., Xu, J., 2022. Evaluating the role of SARS-CoV-2 target genes based on two nucleic acid assay kits. Front. Public Health 10, 982171.